2010

Development of a Multi-Stage Axial Flow Cyclone

Ta-Chih Hsiao
Washington University in St. Louis

Da-Ren Chen
Washington University in St. Louis, chen@me.wustl.edu

Lin Li
Washington University in St. Louis

Paul Greenberg
NASA-Glen Research Center, Cleveland, Ohio, USA

Kenneth W. Street
NASA-Glen Research Center, Cleveland, Ohio, USA

Aerosol Science and Technology, 44:253–261, 2010

ISSN: 0278-6826 print / 1521-7388 online
DOI: 10.1080/02786820903575394

Development of a Multi-Stage Axial Flow Cyclone

Ta-Chih Hsiao,[1] Da-Ren Chen,[1] Lin Li,[1] Paul Greenberg,[2] and Kenneth W. Street[2]

[1]*Department of Energy, Environmental and Chemical Engineering, Washington University in St. Louis, St. Louis, Missouri, USA*

[2]*NASA-Glen Research Center, Cleveland, Ohio, USA*

A prototype multi-stage cyclone system consisting of an impaction inlet and five axial flow cyclone stages has been developed to classify simulants of Lunar and Martian dusts for various research and development needs of NASA's space exploration missions. Individual axial flow cyclone stages can be either independently operated with an inline connection to other particle devices or cascaded together for particle separation and collection. The impaction inlet and first three cyclone stages were designed to operate at the flowrate of 50 lpm under pressure close to ambient. The last two cyclone stages were designed to operate under low pressure conditions to separate particles with diameters less than 200 nm. Due to the limited vacuum capacity of the pump used, the flowrates of last two cyclone stages were restricted to 11.0 and 1.0 lpm when operating the assembled prototype. The impaction inlet and each cyclone stage of the prototype were experimentally calibrated, and the cutoff particle sizes were 11.3 μm, 0.97 μm, 550 nm, 255 nm, 109 nm, and 40 nm.

It was further found that in general the flow Reynolds (*Re*) and particle Stokes numbers (*StK*) were critical parameters to characterize the performance of the axial flow cyclone stages, and the relationship between *Re* and the dimensionless cutoff size ($\sqrt{StK}$) was established. In addition, the collection efficiency curves are shifted to a smaller size range with a decrease of the cyclone pressure. However, using $\sqrt{StK}$ as the abscissa and keeping the same *Re*, the particle collection curves at different pressures can be merged into one. This study also found that the upstream pressure should be used to calculate *StK* instead of the average of upstream and downstream pressures of the test cyclone stage.

1. INTRODUCTION

Long-term human habitation on the Moon and Mars is one important vision for NASA's space exploration program. However, the environments on the Lunar and Martian surfaces are often dusty. In dust samples returned by Apollo and other Lunar missions, about 25 wt% of the lunar regolith is less than 20 μm, and is composed of sharp fragments of broken glass, basalt fragments, and agglutinates (Johnson et al. 1992). The lunar dust could cause severe problems for life support equipment in space, such as seal failure, material abrasion, and vision obscuration. Further, it is the potential to produce adverse physiological effects in human respiratory systems (Gaier 2005). John Young, Apollo 16 astronaut, cautioned that ". . . dust is the number one concern in returning to the moon."

To develop of equipment and systems for in NASA's exploration missions, and to research the health effects of the dust, simulants of Lunar and Martian dusts are generally used. Various dust effects on hardware and biological systems generally depend on particle size, and the size distribution of Lunar and Martian dust simulants covers a wide range. To evaluate the effects of these, a reliable and efficient device is needed to classify and collect the simulants into different size bins, ranging from 20 μm to ultrafine particle. Based on discussions with researchers at NASA Glen Center, it was proposed to separate the simultants into six nominal particle size bins, with lower cutoff sizes at 10 μm, 1 μm, 500 nm, 250 nm, 100 nm, and 40 nm.

Two kinds of technology are available for power separation: sieving or screening, and inertial separation. Sieving has the advantage of setting a sharp upper limit on particle size, but the process is slow and inefficient for particles with sizes smaller than 20 μm (Sung et al. 2007). For inertial separation, the general mechanism is to utilize the force balance between gravitational or centrifugal force and fluid drag. Inertial separation techniques are usually applied to airborne particles in the super-micrometer and upper sub-micrometer size ranges. Cyclones are well-known centrifugal counter-flow air classifiers, widely used as particle collectors in a variety of industrial sectors because of their reliable performance and low operational and maintenance costs. More, cyclones are less prone to particle bounce and overloading, making them suitable for long-term particle collection.

To classify different particle sizes at the same time, a five-stage cyclone system has been developed for in-situ sampling (Smith and Wilson 1979). In this device, tangential cyclones were employed for every stage. However, due to the

Received 10 June 2009; accepted 11 November 2009.

The authors appreciate the financial support of the multi-stage axial flow cyclone development provided by NASA Glen Research Center under contract NNX07AN27G. Mr. Hsiao would also like to acknowledge the financial support of the Ph.D. student scholarship program of the McDonnell International Scholars Academy at Washington University in St. Louis.

Address correspondence to Da-Ren Chen, Department of Energy, Environmental and Chemical Engineering, Washington University in St. Louis, St Louis, MO 63130, USA. E-mail: chen@me.wustl.edu

perpendicular arrangement of the inlet and outlet of tangential cyclone stages, the overall configuration of the five-stage cyclone system is rather bulky and complex. In addition to the tangential cyclone design, axial flow cyclones have been proposed, in which the aerosol flow enters and exits the cyclone body axially. The swirling vortex motion for separating particles in an axial flow cyclone is generated by a helix channel or a spindle vane. The primary advantage of axial flow cyclones is on the relative ease of connecting them with other devices in line. Therefore, the coaxial flow cyclone design simplifies the overall cyclone system configuration and allows the particle-laden stream in a multi-stage cyclone of this type to cascade through individual axial flow cyclone stages. Liu and Rubow (1984) first developed a five-stage cascade axial flow cyclone operated at 30 lpm. The smallest cutoff particle size of this cyclone was 1.05 μm. Further, no model was established for Liu and Rubow's cascade axial flow cyclone.

In this article we report on a new multistage axial flow cyclone developed for the separation of NASA Lunar and Martian dust simulants. The cyclone consists of one impaction inlet stage for particles with sizes larger than 10 μm, and five axial cyclone stages with lower cutoff sizes of 1.0, 0.5, 0.25, 0.1, and 0.04 μm. The flowrate of the impaction and first three stages of the prototype was 50 lpm. By operating the last two cyclone stages at low pressure, cutoff sizes of 0.1 and 0.04 μm were achieved. Further, an empirical model for the cutoff particle sizes of the axial flow cyclone stages was established in this study.

2. AXIAL FLOW CYCLONES

Compared to tangential flow cyclones, limited experimental data and models have been reported for axial flow cyclones. Vaughan (1988) developed simple axial flow cyclones consisting of a helix channel, a 10 mm cylindrical body, and a flow outlet tube in each cyclone. Six different cyclone configurations, with three body lengths and two channel depths, were tested under aerosol flowrates ranging from 1.1 to 4.16 lpm. The cutoff sizes (d_{50}, defined as the particle size at 50% collection efficiency) of the tested cyclones varied between 1.25 and 6.5 μm. The study found poor correlation between the particle cutoff sizes and the flow Reynolds number based on the inlet dimension. Vaughan thus used an empirical method proposed by Chan and Lippmann (1977) to describe particle penetration as a function of particle size. He also claimed that axial flow cyclones could separate particles of smaller diameter and have higher pressure drop than tangential flow cyclones of comparable sizes. The superior performance of axial flow cyclones was explained by three co-existing concentric vortexes in the cyclone body.

Nieuwstadt and Dirkzwager (1995) investigated another type of axial flow cyclone for removing liquid droplets from a gas/liquid stream. The difference between their cyclone and Vaughan's was in the outlet design. To prevent droplets from breaking up during the separation process, a bored-through outlet design was applied. Only the downward vortex was generated in the cyclone body. As a result, the droplet collection efficiency of their cyclones was low, the particle laden flow was less disturbed, and the pressure drop was smaller than that of tangential flow cyclones. These observations on axial flow cyclones are different from Vaughan's conclusions. Nieuwstadt and Dirkzwager also developed a model utilizing a simple time-of-flight concept to estimate the particle penetration through the cyclones, and calculated the pressure field along the cyclone wall.

To predict the particle penetration of an axial flow cyclone under laminar flow (i.e., a helix channel Reynolds number less than 2000), Maynard (2000) proposed a mathematical model. The model assumed the particle separation occurred in the vane section/helix channel and in the cyclone body. To estimate the particle penetration in the vane section, the radial displacement of particles was evaluated with the implicit assumption of no particle mixing at any cross section of the helix channel. A method similar to that used by Nieuwstadt and Dirkzwager (1995) was applied to calculate the particle collection in the cyclone body. However, the overall equation for calculating the total particle penetration through an axial flow cyclone is not explicit, requiring numerical iteration schemes to obtain the penetration given an input condition. Brunazzi et al. (2003) tested axial flow cyclones of three types experimentally and developed a different time-of-flight model to predict their particle separation efficiencies. The model is based on the approach of Litch (1980), with two hypotheses, one assuming complete radial mixing, and the other assuming the absence of radial mixing. By comparing the theoretical calculation to the experimental data, it is shown that complete radial mixing is more realistic than no mixing under their tested conditions.

For removing nanoparticles by cyclones, Tsai et al. (2004) first investigated the performance of the axial flow cyclone under low pressure conditions. The geometric configuration of the tested axial cyclones was similar to that of Vaughan (1988), except that the helix channel used in Vaughan's cyclone was replaced by a turning vane. The experimental results reveal the cutoff size decreased with decreasing pressure in the cyclone body, because less air drag force was imposed on particles under low pressure. The cutoff size approached 43.3 nm when the pressure was reduced to 6 torr in the cyclone body. A semi-empirical model was also developed to model the particle collection efficiency of the test axial flow cyclones. In the model, the particle penetration in the vane section was based on Maynard's expression, and the particle collection in the cyclone body was estimated by applying the same expression to the empirical estimation of the total particle transit time in the cyclone body. The work further reports the effect of the annular Reynolds numbers (using the annular spacing between the cyclone wall and outlet as the characteristic length) on the cutoff particle size at 50% penetration. In addition, Hsu et al. (2005) found that for particle aerodynamic sizes less than 40 nm and at low Peclet numbers the collection efficiency of Tsai's axial flow cyclone could increase as the particle diameter decreases. They hypothesized the above observation was due to particle diffusion deposition, and

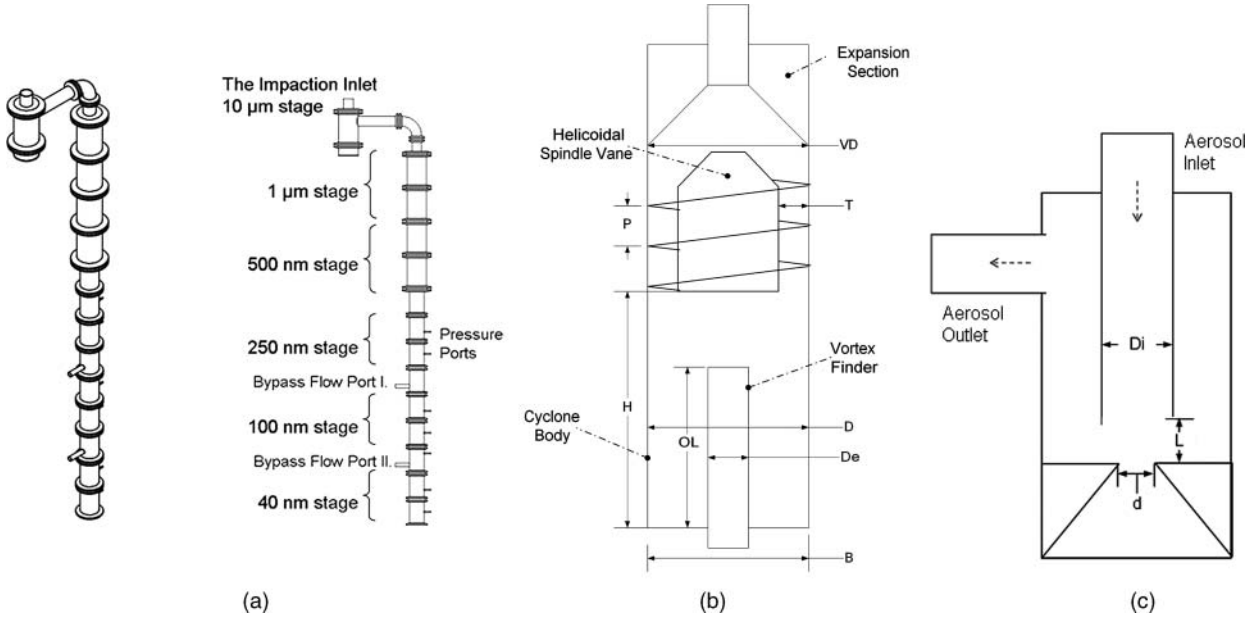

FIG. 1. (a) Schematic diagram of the overall system of the prototype. (b) Schematic diagram of an axial flow cyclone stage (Stages #1–5). (c) Schematic diagram of the impaction inlet.

the simplified convection-diffusion equation was solved analytically for two extreme conditions (i.e., the centrifugal force and the diffusion dominant cases).

3. DESIGN OF THE MULTI-STAGE AXIAL CYCLONE

A schematic diagram of the prototype multi-stage axial flow cyclone is shown in Figure 1. The prototype consists of one impaction inlet and five axial flow cyclone stages (Stages #1–5), corresponding to six nominal cutoff particle sizes of 10 μm, 1 μm, 500 nm, 250 nm, 100 nm, and 40 nm, respectively. The cutoff sizes for each stage of the prototype were determined in consultation with NASA Glen researchers. Because of the limited capacity of the primary vacuum pump to be used with the prototype, the nominal operational flowrate was designed to be 50 lpm. For the axial flow cyclone stages, a design similar to Vaughan's and Tsai's axial flow cyclones was used (shown in Figure 1b). Basically each cyclone stage is comprised of four components: an expansion section, a helicoidal spindle vane, a cyclone body with rectangular base, and a vortex finder/outlet tube. The configuration providing the best particle collection performance was finalized after a series of evaluations with various configurations (Hsiao et al. 2009). The aerosol stream enters each cyclone stage at the top inlet and is smoothly introduced into the vane section. The helicoidal channel in the vane section alters the direction of the axially incoming aerosol stream and generates vortexes in the cyclone body for particle separation and collection. In the cyclone body, particles first flow in the outer vortex and continue to the inner vortex from the end of the outer vortex. The inner vortex spirals upward and exits the cyclone body through the vortex finder (outlet tube) to the following cyclone stage. Operating differently from Stages #1–5, the system inlet, shown in Figure 1c, is in fact the impactor. To increase the dust loading capacity of the impaction stage of the impactor, a small hole connected to a dust collection chamber is centered on the impinging plate. A similar design had earlier been used to increase particle loading capacity and to alleviate particle bounce from the existed impactor (Biswas and Flagan 1988). Critical dimensions of all the stages in the prototype are listed in Table 1. Note that, due to the limited capacity of the vacuum pump used, the last two cyclone stages were forced to operate at reduced aerosol flowrates of 11.0 and 1.0 lpm for Stages #4 and #5, respectively. This reduction was needed because the last two cyclone stages must operate at low pressure to achieve the desired particle cutoff sizes less than 200 nm.

4. EXPERIMENTAL SETUP FOR INDIVIDUAL STAGE CALIBRATION

The performance of the prototype multi-stage cyclone was characterized by the particle collection efficiencies of the stages included. The collection efficiency (η) is defined as

$$\eta = 1 - \frac{C_{down}}{C_{up}},$$

where C_{down} and C_{up} are downstream and upstream particle concentrations. The efficiency curve of each stage was calibrated individually by measuring the upstream and downstream particle size distributions for each stage. The pressure drop across each stage was monitored by a MKS Barometric pressure gauge (626A13TAE, 1000 torr max or 626A11TAE, 10 torr

TABLE 1
Dimensions of the impaction inlet and each cyclone stage of the prototype

Stage	Impaction inlet	Stage	#1	#2	#3	#4	#5
Nominal d_{50}	10 μm	Nominal d_{50}	1 μm	500 nm	250 nm	100 nm	40 nm
Impacting Length (L)	1.106 cm	Pitch (P)	0.675 cm	0.437	0.357	0.278	0.278
Dust Bin Hole (d)	1.106 cm	Channel Depth (T)	0.814 cm	0.457	0.378	0.378	0.378
		BodyDia.(D)*	4.169 cm	4.169	2.899	2.899	2.899
		Body Length (H)	7.620 cm	7.620	5.842	5.842	5.842
		Outlet Length (OL)	4.970 cm	4.970	3.810	3.810	3.810
		Outlet Dia.(De)	0.953 cm	0.953	0.635	0.635	0.635

*The vane diameter (VD) and the base diameter (B) are equal to the body diameter (D).

max). The experimental setup shown in Figure 2 was used to calibrate the cyclone performance. The particle generation system was immediately upstream of a tested stage, and the measurement systems for particle concentration or particle size distribution were immediately downstream. Since the cutoff particle sizes of the prototype ranged from 40 nm to 10 μm, different particle generators and various particle sizing/counting instruments were used in the calibration of individual stages.

In this study, four different particle generation systems (PGS) were employed to produce monodisperse or polydisperse particles in sizes ranging from supermicrometer to nanometer. PGS1 is an ultrasonic particle generator (Sono-Tek 8700) with solution fed by a syringe pump (Harvard 70-2000). PGS1 produced polydisperse potassium chloride (KCl) particles in the supermicrometer range. The ultrasonic nozzle was operated at 120 kHz. The number mean diameter (NMD) of produced particles was about 8 μm using KCl solution of 2.5% by volume. PGS2 is a fluidized bed aerosol generator (FBAG, TSI Model 3400A), and it dispersed Arizona fine dust (Powder Technology Inc. 12103-1 A2) in air as challenge particles. The airborne aerodynamic size distribution of the Arizona fine dust had a mode size of around 1 μm and a geometric standard deviation (GSD) of 1.51. PGS3 includes a homemade Colision atomizer and an electrical classifier with a long DMA (TSI Model 3081). It was used to produce monodisperse KCl particles having electrical mobility sizes from 60 to 500 nm. For particles smaller than 60 nm, the homemade Colision atomizer and the long DMA were replaced by a tube furnace (Linburg/Blue Model 55322) and a Nano-DMA (TSI Model 3085) in PGS4 to generate monodisperse KCl particles. The ratio of the sheath flowrate to the aerosol in

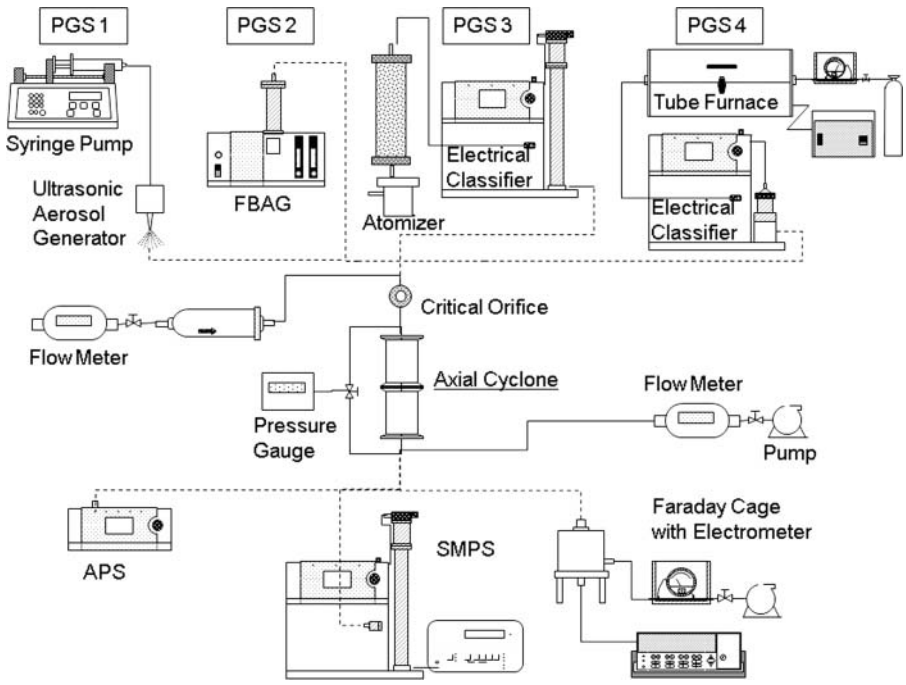

FIG. 2. Schematic diagram of experimental setup for the calibration of the impaction inlet and individual cyclone stages.

the electrostatic classifiers used in PGS3 and PGS4 was kept at 10. Because the operational flowrates of the prototype stages were generally larger than that used to operate the PGSs, filtered dry air was used to make up the flowrate difference between the PGSs and prototype stages. The flowrate of makeup air was monitored and controlled by a mass flow meter (TSI Model 4043) and a needle valve.

Along with four PGSs, two particle sizers and one aerosol counter were applied to measure particle size distribution and concentration, respectively. For particles in the supermicrometer range, an Aerodynamic Particle Sizer (APS, TSI Model 3021) was used to measure particles with diameters ranging from 0.5 to 20 μm (aerodynamic size). A Scanning Mobility Particle Sizer (SMPS, TSI Model 3936) with a DMA (TSI Model 3081 or 3085) and ultrafine condensation particle counter (UCPC TSI Model 3025) was used to measure particles in sizes from 10 to 700 nm (electrical mobility size). Since cyclones separate particles based on aerodynamics, the electrical mobility size (d_e) classified by SMPS was converted to the aerodynamic particle size (d_a) based on the formula given by Hinds (1998):

$$d_a = d_e \left(\frac{1}{\chi} \frac{\rho_p}{\rho_0} \frac{C_c(d_{ve})}{C_c(d_a)} \right)^{0.5},$$

where $C_c(d_{ve})$ and $C_c(d_a)$ are the respective Cunningham slip coefficients for the volume equivalent size (d_{ve}) and the aerodynamic particle size (d_a), χ is the particle shape factor, ρ_p is the particle density, and ρ_0 is the density of 1000 kg/m^3. For spherical particles, d_e is equal to d_{ve}. The shape of KCl particles generated by solution atomization is relatively spherical compared with the cubic morphology of NaCl particles. The shape factor of 1.05, reported by Horvath (1974) for cubes with rounded edges, was thus used for the cases of KCl particles larger than 60 nm. The KCl particles generated by condensation using the tube furnace ($d_p < 60$ nm) were nearly spherical, and a shape factor is of 1.0 was used to convert the electrical mobility size (d_e) to the aerodynamic particle size (d_a). Further, the Arizona fine dust used in PGS2 is not spherical. A shape factor of 1.5 and a density of 900 kg/m^3 were used to correct the APS data, based on the expression reported by Brockmann and Rader (1990) for the APS response for nonspherical particles.

The operational pressure of the last two stages of the prototype was below 200 torr. Unfortunately, the SMPS system described above was unable to operate at such low pressure due to the UCPC limit. Monodisperse particles produced by PGS3 and PGS4 were therefore used to evaluate the performance of the last two stages of the prototype. Since particles classified by DMAs are electrically charged, a homemade Faraday cage with a sensitive electrometer (Keithley Model 6514) was utilized to measure the current carried by the test particles. The particle concentration was then derived from the measured current with the given volumetric sampling flowrate and average electrical charges on DMA-classified particles. The majority of the DMA-classified particles in the test size range in fact carry only one electrical charge (Wiedensohler et al. 1986). Further, the fraction of multiply-charged particles was minimized by selecting particles of desired sizes from the right-hand side of the particle size distribution peak. In this way, the concentration ratio of the doubly charged particles to the singly charged ones is less than 0.05, and the ratio for multiply charged particles was even less. Prior to their use in the calibration, we also verified the average charges on DMA-classified particles by measuring the current carried by the particle stream with the Faraday cage and the particle concentration with a UCPC at ambient pressure.

The penetration curves of different stages of the prototype were determined by the combination of the above described PGSs and the particle sizing/counting instruments. The calibration setup for each stage is listed in Table 2. The vacuum pump (Leybold Vacuum, Trivac B. Rotary Vane Vacuum Pump, D65B) with a needle valve was used to control the flowrate needed during the calibration. Since the performance of cyclone stages with a particle cutoff sizes less than 200 nm (i.e., Stages #4 and #5) was strongly correlated with the pressure level in the stage body, the orifices of different diameters were utilized to achieve the desired pressure conditions. A MKS Baratron type pressure gauge (626A13TAE, 1000 torr max and 626A11TAE, 10 torr max) was used to measure the absolute pressure before the vane section (upstream pressure) and after the test cyclone stage (downstream pressure). The impaction inlet and Stages #1–3 were calibrated at an aerosol flowrate of 50 lpm (at STP conditions) and at near ambient pressure. Stage #4 was calibrated at a flowrate of 20.0 lpm (at STP conditions) under upstream pressures of 274 and 319 torr to investigate the effect of pressure, and Stage #5 was calibrated at flowrate of 1.0 lpm (at STP conditions) under upstream pressures of 21.8 torr. However, due to the limited load capacity of the vacuum pump used, Stage #4 was operated at the flowrate of 11.0 lpm (instead of at 20.0 lpm) to approach the designated particle cutoff size of 100 nm. Details of the operation of Stages #4 and #5 will be given in the following section.

TABLE 2
Experimental setups for the individual calibration of the impaction inlet and cyclone stages

Stage	Impaction inlet	#1	#2	#3	#4	#5
Aerosol Generator	PGS1	PGS2		PGS3		PGS4
Sizing or Counting Apparatus	Aerodynamic Particle Sizer		SMPS	Faraday Cage with Electrometer		

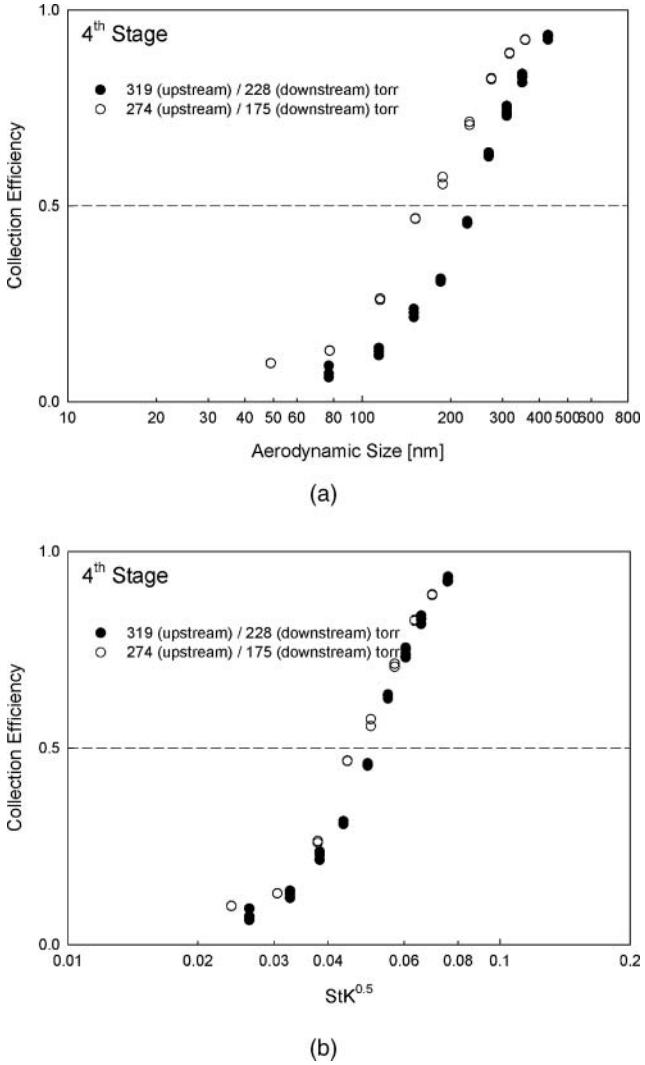

FIG. 3. Particle collection efficiency curves for the 4*th* cyclone stage under two different pressure conditions (i.e., 319 torr and 274 torr) at 20 lpm. (a) aerodynamic size as the abscissa; (b) square root of *StK* number as the abscissa.

5. RESULTS AND DISCUSSION

Tsai et al. (2004) have demonstrated that the cutoff size (d_{50}) of an axial flow cyclone decreases with decreasing cyclone inlet pressure. As shown in Figure 3a, similar behavior was observed in our prototype. The d_{50} of Stage #4 decreased from 229 to 161 nm as the upstream pressure was reduced from 319 to 274 torr at 20 lpm (at STP conditions). Since cyclones utilize centrifugal force and particle drag to separate particles, the fact that d_{50} decreased with upstream pressure can be explained by the smaller drag experienced by a particle at the lower pressure. This effect is also described in the slip coefficient (C_c) of the particle Stokes number (*StK*). Reduction of the cyclone upstream pressure increases the mean free path (i.e., λ) of the carrier gas and the particles' Knudsen number (*Kn*), defined as $2\lambda/d_p$, consequently resulting in larger values of C_c and *StK* for particles of the same diameter. As a result, the cyclone can capture smaller particles under the lower pressure condition.

$$StK = \frac{C_c \rho_p d_p^2 V_i}{9\mu D_c}, \text{ and}$$

$$C_c = 1 + Kn \cdot \left[1.257 + 0.400 \cdot \exp\left(-\frac{0.55}{Kn}\right)\right],$$

where ρ_p is the particle density, V_i is the average flow velocity in the vane section, μ is the fluid viscosity and D_c is the cyclone body diameter.

However, when these two collection efficiency curves were re-plotted using the square root of the particle *StK* number as the abscissa, the curves at two different operational pressure levels collapse into one (Figure 3b). In other words, the characteristic cutoff Stokes number (StK_{50}) of an individual cyclone stage does not change with the cyclone's operational pressure under the same STD flow rate (the same flow Reynolds number). Note that Tsai et al. (2004) applied the average of upstream and downstream cyclone pressures for the *StK* number calculation. Different from the observation of Tsai et al. (2004), we found the *StK*, C_c, and *Kn* better correlate the curves under different pressures when calculated based on the upstream pressure of an individual cyclone stage.

In addition to Stage #4, the particle collection efficiency curves for all the other stages of the multi-stage cyclone prototype were calibrated individually and are plotted in Figure 4. Similar S-shape collection efficiency curves were observed for all the stages. The corresponding aerodynamic cutoff sizes, the tested flow rate, and the pressure conditions are summarized in Table 3. In general, the experimental cutoff sizes are reasonably close to the nominal designed cutoff size, except the cutoff sizes of Stages #3 and #4. Therefore, to approach the nominal cutoff sizes, in the assembled prototype theses two stages were operated at lower pressures than those of the separately calibrated conditions. Details of flow operation scheme will be described in a later section.

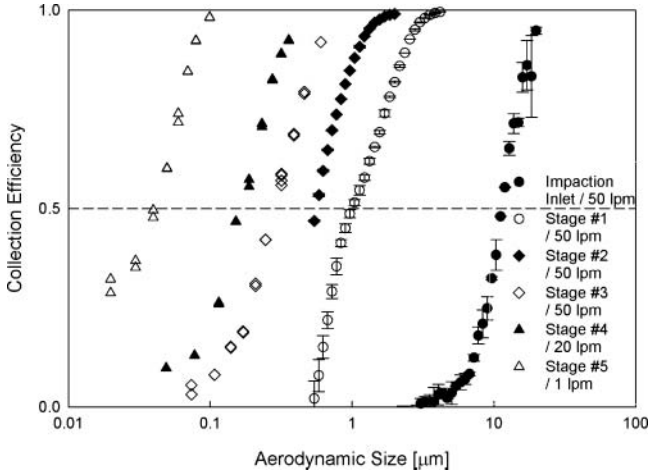

FIG. 4. Measured collection efficiency curves of the impaction inlet and individual cyclone stages of the prototype.

TABLE 3
Experimental cutoff particle sizes of the impaction inlet and cyclone stages (Note that two orifice plates were installed in the assembled cyclone prototype to regulate the upstream pressures of Stages 4 and 5: one is between Stages 3 and 4 and the other between Stages 4 and 5)

Stage	Nominal d_{50}	Test flowrate*	Upstream pressure	Downstream pressure	Re#	Experimental d_{50}
Impaction Inlet	10 μrn	50 lpm	760 torr	760 torr	3046	11.3 μrn
#1-1	1 μm	50 lpm	760 torr	760 torr	41499	1 μm
#1-2	1 μm	20 lpm	760 torr	760 torr	16600	1.87 μm
#2	500 nm	50 lpm	760 torr	760 torr	114241	550 nm
#3	250 nm	50 lpm	760 torr	578 torr	117488	290 nm
#4-1	100 nm	20 lpm	319 torr	228 torr	60423	229 nm
#4-2	100 nm	20 lpm	274 torr	175 torr	60423	161 nm
#5	40 nm	1 lpm	21.8 torr	6.7 torr	3021	40.9 nm

*These flowrates are under STP conditions.

The steepness of these collection curves was characterized by the square root of the ratio of particle size with 84% collection efficiency to that with 16% efficiency. The larger the value, the less sharp the collection curve. A value of 1.0 indicates the ideal cutoff curve as a step function. For the impaction inlet, the steepness of the cutoff curve is about 1.43. The values of cyclone Stages #1–4 were higher, ranging between 1.70∼1.90. Because of the diffusion of small particles, Stage #5 had the least sharp particle collection efficiency, exhibiting a slightly high collection value in the smaller particle size range. The steepness of the collection curve for Stage #5 was thus decreased to 2.35. This phenomenon was also observed in the work of Hsu et al. (2005). Compared with the values ranging from 1.08 to 1.10 for a MOUDI (Microorfice Uniform Deposit Impactor), the steepness values of the cyclone cutoff curves are in general large. However, the advantage of the multistage cyclone prototype over impactors is in its loading capacity, which is much higher than that of a MOUDI. The high particle loading capacity and low pressure drop of cyclones make them more appropriate for collecting particles at high concentration and high flowrates.

Similar to the normalized process applied for the collection curves of Stage #4, the different particle collection efficiency curves of axial flow cyclone stages were re-plotted by replacing the aerodynamic particle size with the square root of the Stokes number ($\sqrt{StK}$), which is also considered to be a dimensionless particle size. As seen in Figure 5, the efficiency curves of different stages overlap somewhat, but do not exactly converge into one characteristic collection efficiency curve. In addition, the dimensionless cutoff sizes ($\sqrt{StK_{50}}$) of different cyclone stages are not the same. It is because of the different geometric dimensions, such as the cyclone body diameter, and different operational conditions, such as the flow velocity, in the stages. To characterize the performance of different axial flow cyclone stages, the $\sqrt{StK_{50}}$s were further plotted against the flow Reynolds number (*Re*). The *Re* number are defined as

$$Re = \frac{\rho_g V_i D_c}{\mu},$$

where ρ_g is the carry fluid density.

As shown in Figure 6, the $\sqrt{StK_{50}}$ decreased with increasing *Re#*. Further, the slope of the $\sqrt{StK_{50}}$ vs. *Re#* curve decreased in the higher *Re#* regime. This observation was previously reported for tangential flow cyclones (Moore and McFarland 1990; Scarlett 1987; Overcamp and Scarlett 1993; Lidén and Gudmundsson 1997). Overcamp and Scarlett (1993) further concluded that the $\sqrt{StK_{50}}$ generally falls between 0.025 and 0.05 for a tangential flow cyclone operating under high Reynolds number ($Re > 10^5$), and they suggested values within this range can be chosen as the preliminary $\sqrt{StK_{50}}$ for designing a new industrial tangential cyclone. Note that the definition of the *StK* given in Overcamp and Scarlett (1993) is different from that used in our study, and the proposed *StK* range will need to be revised if the current definition of the *StK* is used. The work further cautioned that the correlation between $\sqrt{StK_{50}}$ and *Re* is strongly related to the cyclone configurations. Since the stages of the prototype axial flow cyclone have similar geometric dimensional ratios, an empirical quadratic equation was established to express the correlation between $\sqrt{StK_{50}}$ and *Re*, for *Re* up to $1.2*10^5$. The cutoff size of an axial flow cyclone with a similar dimensional

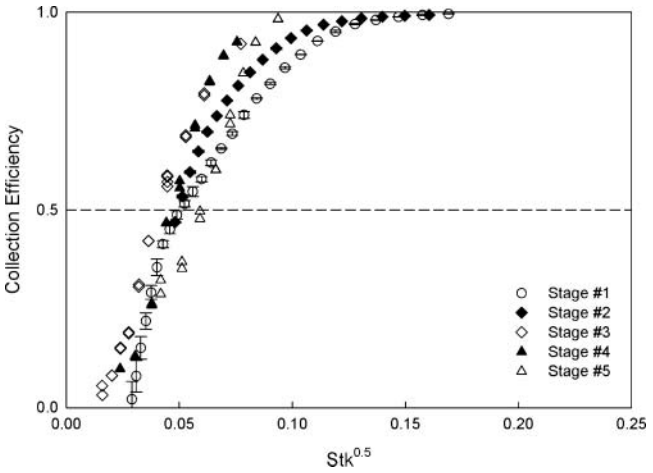

FIG. 5. Collection efficiency curves as a function of the particle Stokes number for all the axial flow cyclone stages of the prototype.

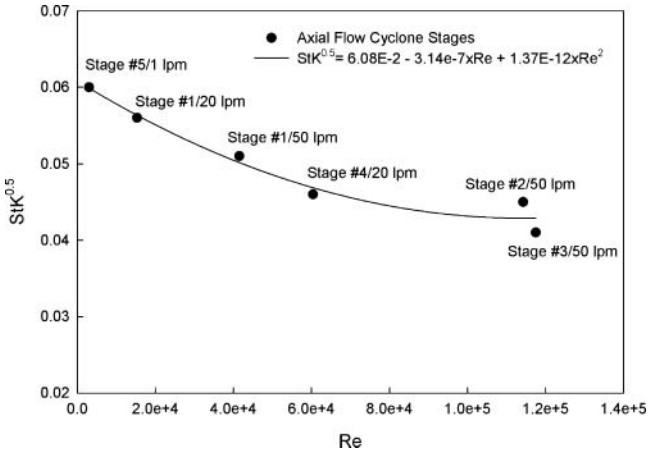

FIG. 6. Dimensionless cutoff size ($StK_{50}^{0.5}$) vs. flow Reynolds number for all axial flow cyclone stages.

ratio can therefore be estimated by this empirical model under different Reynolds numbers. When Re is larger than $1.2*10^5$, the $\sqrt{StK_{50}}$ can be assumed to be a constant value of 0.043. Expressed mathematically,

$$\sqrt{StK_{50}} = 6.083 \cdot 10^{-2} - 3.142 \cdot 10^{-7} \cdot Re + 1.375 \cdot 10^{-12} \cdot Re^2, \text{ for } 0 < Re < 1.2 \cdot 10^5.$$

The experimental data reported above are for the impaction inlet and cyclone stages calibrated individually at the designed flowrates.

Because the pressure conditions and the flowrates for the Stages #3 and #4 are not identical to those in the individual stage calibration, additional calibration was also done on the assembled prototype. The flowrate of Stage #3 remained at 50 lpm in the assembled prototype, but the upstream pressure of the stage decreased to 660 torr due to the pressure drop caused by the previous stage. Hence the cutoff size of Stage #3 decreased from 290 nm to 255 nm. For Stage #4 to meet the requirement of the nominal cutoff size of 100 nm, the upstream pressure needed to be reduced to 200 torr at 20 lpm, based on the result obtained in individual stage calibration. However, because of the limited loading capacity of the vacuum pump used, Stage #4 was forced to operate at the flowrate of 11.0 lpm in the assembled prototype, instead of at 20 lpm. An orifice with a diameter of 0.16 mm was installed in front of the vane section of Stage #4. With the orifice installed, the upstream pressure of Stage #4 was thus decreased to 141.5 torr, and the cutoff size thus became 109 nm. Figure 7 shows the overall calibration result and the flow operation scheme for the assembled prototype.

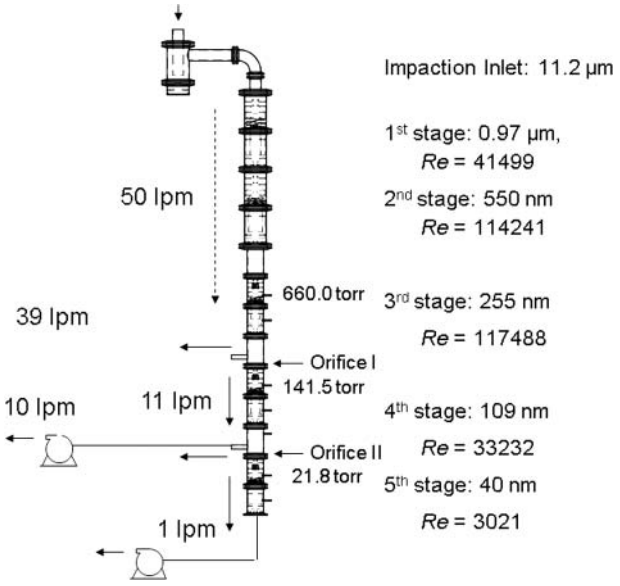

FIG. 7. Overall flow operation scheme of the prototype and the corresponding cutoff sizes for the impaction inlet and cyclone stages.

To maintain different flowrates for cyclone Stages #4 and #5, two small vacuum pumps with critical orifices were connected to remove excess aerosol flow from the assembled prototype. In addition, orifices with a diameter of 0.16 mm were also installed before the last axial flow cyclone stages to reduce the cyclone upstream pressure to the expected level. Since aerosol flow is restricted by the critical orifices, the particle loss is in general expected. However, the experimental study by Chen et al. (2007) has shown that the particle loss through a 0.23 mm critical orifice under the choked flow condition is less than 3.5% for particle sizes larger than 15 nm. It is thus believed the particle losses in these two orifices are negligible.

To date, only two multi-stage cyclones have been reported. One is a five-stage tangential flow cyclone operated at 28.3 lpm, designed by Smith and Wilson (1979). The other one is a five-stage cascade axial flow cyclone operated at 30 lpm, developed by Liu and Rubow (1984). The smallest cutoff particle sizes in these two cyclones were 0.32 and 1.05 μm, respectively. Compared with these multi-stage cyclones, the prototype operated under a higher flowrate of 50 lpm, covered a wider cutoff size range, and collected particles of smaller sizes. As expected, the smaller cutoff particle size of the prototype resulted in a higher pressure drop than that reported for the Smith and Wilson cyclone (i.e., 170.2 torr). However, comparable performance under a higher operational flowrate was achieved by our prototype if Stages #4 and #5 were not used. For the Liu and Rubow cascade axial cyclone, no pressure data was published.

6. CONCLUSIONS

A prototype multi-stage cyclone system having an impaction inlet and five axial flow cyclone stages with cutoff sizes of 11.3 μm, 0.97 μm, 500 nm, 255 nm, 109 nm, and 40 nm has been developed to classify Lunar and Martian dust simulants for various NASA research and development work. To calibrate the impaction inlet and cyclone stages, four different particle generation systems (PGS1-4) were used to generate test particles in sizes ranging from tens of micrometers down to several nanometers. Two particle size spectrometers (APS and SMPS)

and an aerosol electrometer (consisting of a Faraday cage with a sensitive electrometer) were applied to measure the particle size distribution and concentration upstream and downstream of the impaction inlet and of each cyclone stage of the prototype. The calibration of each cyclone stage was done at the designed flowrate condition. The experimental cutoff sizes of several cyclone stages deviated slightly from those targeted. However, adjustments to the operational flowrate and pressure of the assembled multi-stage cyclone system brought the cutoff particle sizes of each stage to within 10% of the target sizes. Compared with two existing multi-stage cyclones, i.e., a five-stage tangential flow cyclone (Smith and Wilson 1979) and a five-stage cascade axial flow cyclone (Liu and Rubow 1984), the prototype has the advantages of covering a wider size range and collecting particles of smaller sizes at a higher flowrate. However, due to the lower particle cutoff size, the pressure drop across the prototype was greater than those of the earlier cyclones mentioned. Nevertheless, without Stages #4 and #5, the performance and pressure drop of the prototype were comparable to those of Smith and Wilson's cyclone system.

The experimental data also reveal that the cyclone collection efficiency curves varied with the operational upstream pressure. The cutoff sizes of Stage #4 decreased with a decrease of upstream pressure, because of less drag force acting on particles in a lower pressure environment. By converting the particle diameter to the square root of the particle Stokes number ($\sqrt{StK}$), the particle collection efficiency curves of Stage #4 under different pressure conditions can be nearly collapsed into one at the same flow Reynolds number (Re). In other words, the pressure effect on the cutoff particle sizes of Stage #4 can be mainly attributed to the change of the slip coefficient (C_c) in the Stokes number. This study found that, to better scale the collection efficiency curves under different pressure conditions, the upstream pressure should be used to calculate the particle Stokes number instead of the average of upstream and downstream pressures of the test cyclone stage. The relationship between the $\sqrt{StK}$ and Re for tangential flow cyclones was also observed for axial flow cyclone stages. For Re less than $1.2*10^5$, the $\sqrt{StK_{50}}$ decreased with an increase of Re. The value of $\sqrt{StK_{50}}$ approached a constant for Re larger than $1.2*10^5$. An empirical model was then derived to describe the correlation between $\sqrt{StK_{50}}$ and Re with the given geometric dimensions of cyclones. The model can be used to predict the cutoff particle sizes for axial flow cyclones with similar dimensional ratios under different flow rates.

REFERENCES

Biswas, P., and Flagan, R. C. (1984). High Velocity Inertial Impactors, *Environ. Sci. Technol.* 18:611–616.

Biswas, P., and Flagan, R. C. (1988). The Particle Trap Impactor, *J. Aerosol Sci.* 19:113–121.

Brockmann, J. E., and Rader, D. J. (1990). APS Response to Nonspherical Particles and Experimental Determination of Dynamic Shape Factor, *Aerosol Sci. Technol.* 13:162–172.

Brunazzi, E., Paglianti, A., and Talamelli, A. (2003). Simplified Design of Axial-Flow Cyclone Mist Eliminators, *AIChE J.* 49:41–51.

Chan, T., and Lippmann, M. (1977). Particle Collection Efficiencies of Air Sampling Cyclones: An Empirical Theory, *Environ. Sci. Technol.* 11:377–382.

Chen, S. C., Tsai, C. J., Wu, C. H., Pui, D. Y. H., Onischuk, A. A., and Karasev, V. V. (2007). Particle Loss in a Critical Orifice, *J. Aerosol Sci.* 38:935–949.

Gaier, J. R. (2005). The Effects of Lunar Dust on EVA Systems During the Apollo Missions, NASA/Glenn Research Center, Cleveland, Ohio. TM—2005–21361.

Horvath, H. (1974). The Sedimentation Behavior of Non-Spherical Particles. *Staub, Reinhaltung der Luft* 34:197–202.

Hsiao, T. C., Chen, D. R., Greenberg, P., and Street, K. W. (2009). Effect of Geometric Configurations on Collection Efficiency of Axial Cyclone, *Particle and Particle System Characterization,* submitted.

Hsu, Y. D., Chein, H. M., Chen, T. M., and Tsai, C. J. (2005). Axial Flow Cyclone for Separation and Collection of Ultrafine Particles: Theoretical and Experimental Study, *Environ. Sci. Technol.* 39:1299–1308.

Johnson, S. W., Taylor, G. J., and Wetzel, J. P. (1992). Environmental Effects on Lunar Astronomical Observatories, *The Second Conference on Lunar Bases and Space Activities of the 21st Century*, NASA. Johnson Space Center 1:329–335.

Licht, W. (1980). *Air Pollution Control Engineering*, Dekker, New York.

Lidén, G., and Gudmundsson, A. (1997). Semi-empirical Modeling to Generalise the Dependence of Cyclone Collection Efficiency on Operating Conditions and Cyclone Design, *J. Aerosol Sci.* 28:853–874

Liu, B. Y. H., and Rubow, K. L. (1984). A New Axial Flow Cascade Cyclone for Size Characterization of Airborne Particle Matter. In *Aerosols*. B. Y. H., Liu, D. Y., Pui, and H. J., Fissan, eds. Elsevier, Amsterdam, 115–118.

Maynard, A. D. (2000). A Simple Model of Axial Flow Cyclone Performance Under Laminar Flow Conditions, *J. Aerosol Sci.* 31:151–167

Moore, M. E., and McFarland, A. R. (1990). Design of Stairmand-Type Sampling Cyclones, *Am. Ind. Hyg. Assoc. J.* 51:151–159

Nieuwstadt, T. M., and Dirkzwager, M. (1995). A Fluid Mechanics Model for an Axial Cyclone Separator, *Ind. Eng. Chem. Res.* 34:3399–3404

Overcamp, T. J., and Scarlett, S. E. (1993). Effect of Reynolds Number on the Stokes Number of Cyclones, *Aerosol Sci. Technol.* 19:362–370

Scarlett, S. E. (1987). *An Investigation of Cyclone Performance Using Dimensional Analysis*. M.S. Thesis, Clemson University, Clemson, SC.

Smith, W. B., and Wilson, R. R. (1979). The Five-Stage Cyclone System for In Situ Sampling, *Environ. Sci. Technol.* 13:1387–1392

Sung, M. D., Dent, N. M., and Kalechofsky, N. (2007). Ultra Fine Particle Size Classification via Sieving in Liquid Nitrogen, *PARTEC 2007 International Congress on Particle Technology*, Nuremburg, Germany, March, 2007.

Tsai, C. J., Chen, D. R., Chein, H. M., Chen, S. C., Roth, J. L., Hsu, Y. D., Li, W., and Biswas, P. (2004). Theoretical and Experimental Study of an Axial Flow Cyclone for Fine Particle Removal in Vacuum Conditions, *J. Aerosol Sci.* 35:1105–1118

Tsai, C. J., Chen, S. C., Przekop, R., and Moskal, A. (2007). Study of an Axial Flow Cyclone to Remove Nanoparticles in Vacuum, *Environ. Sci. Technol.* 41:1689–1685

Vaughan, N. P. (1988). Construction and Testing of an Axial Flow Cyclone Preseparator, *J. Aerosol Sci.* 3:295–305

Wedding, J. B., Welgand, M. A., and Carney, T. C. (1982). A 10-μm Cutpoint Inlet for the Dichotomous Sampler, *Environ. Sci. Technol.* 16:602–606

Wiedensohler, A., Ltkemeier, E., Feldpausch, M., and Helsper, C. (1986). Investigations of the Bipolar Charge Distribution at Various Gas Conditions, *J. Aerosol Sci.* 17:413–416.